GDCh Research Article Angewandte International Edition Chemie www.angewandte.org

Check for updates

How to cite: *Angew. Chem. Int. Ed.* **2025**, e202425601
doi.org/10.1002/anie.202425601

Photocatalysis Hot Paper

Natural Sunlight-Driven Activation of Inert Aryl Halides Using Plasmonic Cu@CdS with Polysulfide Active Sites

Yuemei Li[+], Shi-Yu Guo[+], Hongfei Gu, Bingyu Wang, Peiwu Su, Xiuming Zhang, Haoqing Zhang, Shuping Zhang, Fanzhi Yang, Jia Liu, Qing-An Chen,* and Jiatao Zhang**

Abstract: Visible light photoredox catalysis has become a rapidly emerging area owing to its potential of using sunlight to tame previously hard-to-harness radicals for organic synthesis. At present, such a blueprint faces a significant challenge, namely how to accomplish thermodynamically demanding reactions with sunlight encompassing a wide range of low-energy photons. Here, we report a new reaction framework to overcome this bottleneck through decoupling the thermodynamic limits of photoreduction from photoexcitation. This is fulfilled based on the construction of a heterogeneous photocatalyst Cu@CdS possessing in situ-formed surficial polysulfide species (including $S_3^{\bullet-}$ and S_4^{2-}), which can efficiently harvest solar energy via plasmonic absorption of Cu while manifest sufficient redox potential for activating inert aryl bromides/chlorides enacted by excited polysulfides. We demonstrate that this designed material composes a potent photoredox catalyst for efficient aryl cross-coupling, borylation, hydrogenation, as well as Birch-type dearomatization reactions, with good recyclability and stability. In particular, when exclusively using natural sunlight as an energy source, the product yield can still reach up to 90%. Our findings introduce a straightforward yet viable way to progress toward the century-long dream of leveraging natural sunlight to produce structurally complex organic molecules, just like plants on Earth.

Introduction

About one century ago, the pioneering chemist Giacomo Ciamician put forward a grand vision of constructing complex organic compounds the way that plants do by leveraging abundant and sustainable sunlight as an energy source.[1,2] Considerable strides have been made toward this ambitious synthetic goal in the recent two decades, largely facilitated by the development of visible light photoredox catalysis, which affords access to open-shell radical intermediates via single electron transfer (SET).[3–10] Such a reaction mode bypasses canonical two-electron bond disconnection mechanisms, unlocking possibilities for achieving previously intractable synthetic transformations. Despite significant advances, however, current methodologies come with a notable limitation. That is, the narrowly emitting blue LEDs (400–440 nm) are dominantly utilized as the light source in photoredox catalysis, which does not align well with the principle of solar manufacturing wherein efficient utilization of a large portion of solar flux is in demand.[6,11–15]

The reason for the adoption of blue light irradiation is decided by the photophysical properties of typical photoredox catalysts, and even with such high energy input, the attainable redox potential scope is restricted for bond activation. To overcome the intrinsic conflict between expanding solar light harvesting range and gaining energetic driving force, innovations have been made based on consecutive photoinduced electron transfer ([ConPET], Figure 1a), triplet–triplet annihilation photon upconversion ([TTA-UC], Figure 1b), as well as sensitization-initiated electron transfer ([SenI-ET], Figure 1c), respectively.[2,16–24] In these reaction schemes, longer-wavelength visible light and even near-infrared light can be harnessed to accomplish photoreduction of energy-demanding substrates, such as aryl bromides/chlorides with rather negative reduction potential and high bond dissociation energy.[17,21,25] Nevertheless, they also suffer a variety of limitations, including the necessity of using excessive sacrificial electron donors, the requirement of sophisticated coupling of multiple components in the reaction system, and/or the tendency for the excited photocatalyst intermediates to decompose, etc. Therefore, it is desirable to explore more sustainable and facile protocols that can show large absorption cross-sections over a broad range of the solar spectrum and, at the same

[*] Y. Li[+], H. Gu, P. Su, X. Zhang, H. Zhang, J. Liu, J. Zhang
School of Materials Science and Engineering, School of Chemistry and Chemical Engineering, Beijing Key Laboratory of Construction-Tailorable Advanced Functional Materials and Green Applications, Beijing Institute of Technology, Beijing100081, China
E-mail: liujia86@bit.edu.cn
zhangjt@bit.edu.cn

S.-Y. Guo[+], Q.-A. Chen
Dalian Institute of Chemical Physics, Chinese Academy of Sciences, Dalian116023, China
E-mail: qachen@dicp.ac.cn

B. Wang, F. Yang
Advanced Research Institute of Multidisciplinary Science, Beijing Institute of Technology, Beijing100081, China

S. Zhang
Institute of Materials, Henan Key Laboratory of Advanced Conductor Materials, Henan Academy of Sciences, Zhengzhou450046, China

[+] Both authors contributed equally to this work.

Additional supporting information can be found online in the Supporting Information section

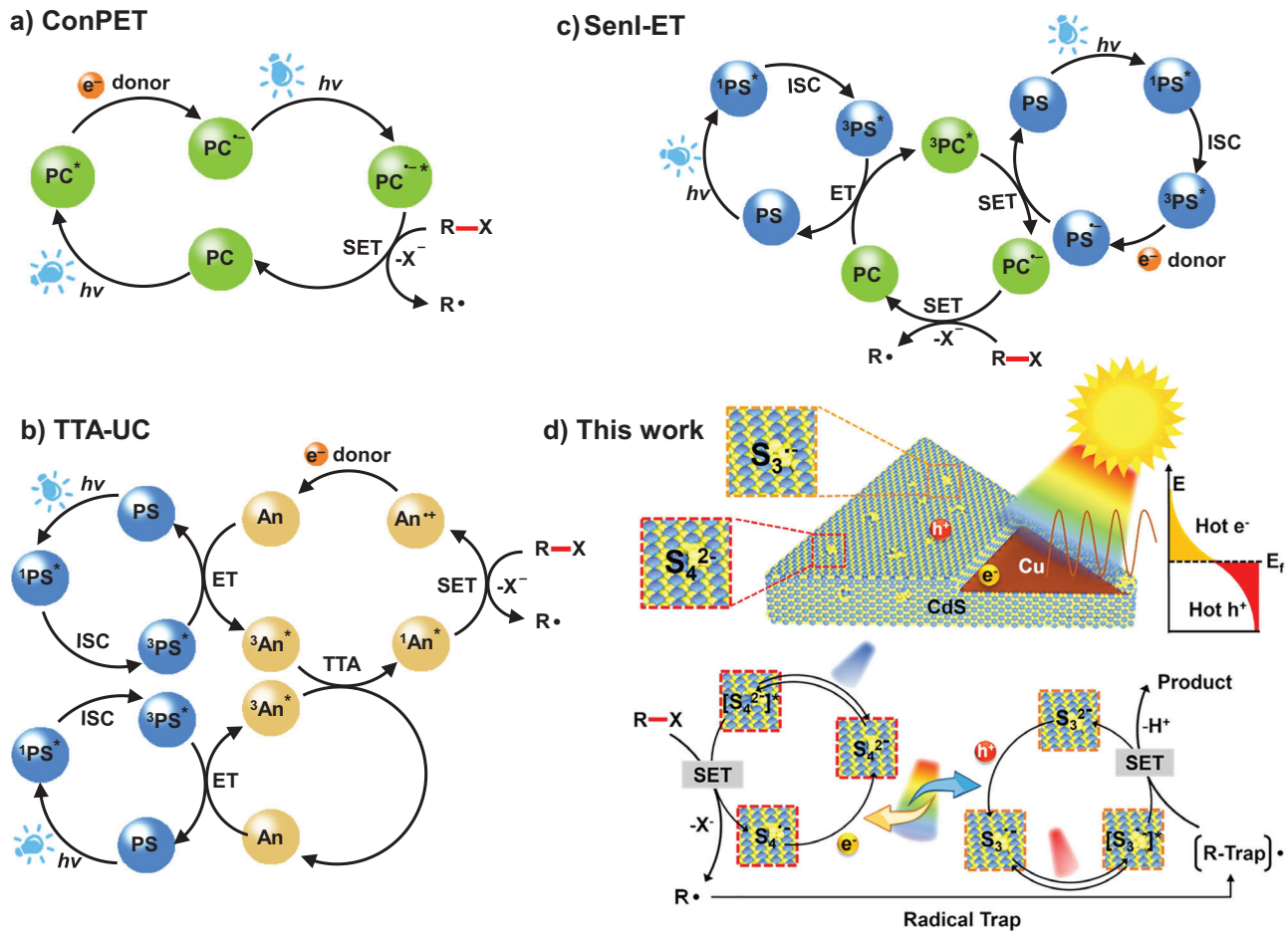

Figure 1. Illustration of the strategies proposed for decoupling the thermodynamic limits of photoreduction from photoexcitation in visible light photoredox catalysis.

time, boast potent redox power capable of activating inert substrates.

In parallel with homogeneous photoredox catalysts like transition metal complexes and organic dyes,[8,9] heterogeneous semiconductors offer an alternative paradigm in photoredox catalysis featuring recyclability, high durability, easy separation of products, and favorable adaptation toward large-scale synthesis.[16,26–30] Particularly, metal chalcogenides, either in bulk or quantum dimension, have been widely studied and shown good performance in many important organic transformations.[26,31–37] A prevalent view is that their photoredox capability directly relies on the conduction and valence band positions. Although new reaction patterns involving Auger recombination or thiyl radials have been proposed very recently,[38,39] a non-innocent element in the elucidation of the whole picture of the reaction mechanism has long been missing.[40] That is, the chemical nature of the surface species that are susceptible to oxidation caused by trapped holes (i.e., photocorrosion) during the photoredox process, and furthermore their reactivity and potential influences on the reaction pathway. Although these issues remain underdeveloped, it is imperative to be decoded in view of the recent discovery of the unique photoredox properties of polysulfide anions in an excited state.[17,41–43] Specifically, Chiba and co-workers revealed that the homogeneous polysulfide anions $S_3^{\bullet-}$ and S_4^{2-} dissolved in DMSO can function as competent visible-light photoredox catalysts for activating strong C–X bonds and inert π-systems. Inspired by these findings, we hypothesize that it may be feasible to create $S_3^{\bullet-}$ and S_4^{2-} active sites on the surface of sulfide semiconductors by exploiting the photocorrosion process. This would enable us to leverage the high redox power of the polysulfide anions upon visible light excitation while simultaneously establishing a heterogeneous catalytic system.

Herein, for getting closer to the longstanding goal of solar manufacturing, a plasmonic Cu@CdS core@shell photocatalyst possessing in situ formed $S_3^{\bullet-}$ and $S_4 2^-$ active sites is fabricated. This heterogeneous photocatalyst not only displays broadband solar light harvesting beneficial from localized surface plasmon resonance (LSPR) of Cu but also enables productive activation of C_{aryl}–Cl and C_{aryl}–Br bonds with elusive redox potentials (Figure 1d). By exploiting natural sunlight as the sole energy input, the catalyst delivers excellent yields of up to 90% in biaryl cross-coupling reactions, such a reaction system is additionally amenable to borylation and hydrogenation of aryl halides, as well as

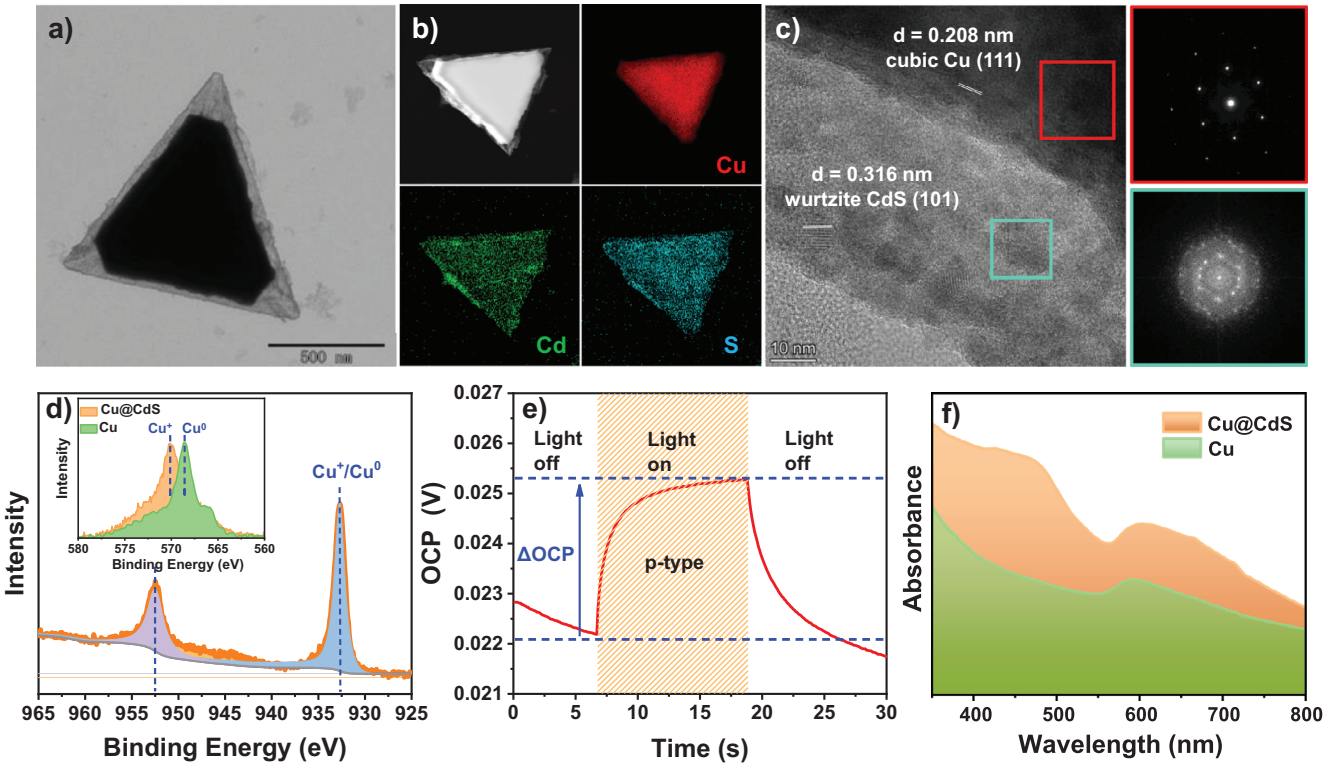

Figure 2. Structural and physicochemical characterizations of Cu@CdS photocatalyst. a) TEM image. b) HAADF-STEM image and corresponding EDX elemental maps for Cu, Cd, and S. c) HRTEM image with FFT patterns corresponding to the areas enclosed by red or green squares. d) Cu 2p XPS spectrum (inset: Cu LMM Auger spectrum). e) Open-circuit potential responses under illumination and in the dark. f) Optical absorption spectrum in comparison with bare Cu triangular prisms.

Birch-type reduction of arenes, giving rise to highly value-added products.

Results and Discussion

Synthesis and Characterization of Photoredox Catalyst

In this work, non-noble metal Cu with strong LSPR comparable to Au and Ag but much reduced cost was exploited as the core material to create the Cu@CdS core@shell photocatalyst (hereafter denoted as Cu@CdS).[44,45] The synthesis was accomplished by partial sulfuration of the starting Cu triangular prisms to yield Cu@Cu_7S_4 core@shell structures (Figures S1–S4), followed by Cd^{2+}-for-Cu^{+} cation exchange under mild reaction conditions.[46–48] The representative transmission electron microscopy (TEM) image of the resultant material is presented in Figure 2a, which clearly denotes the triangular-shaped core@shell configuration. High angle angular dark field-scanning TEM (HAADF-STEM) image in conjunction with energy dispersive X-ray (EDX) elemental mapping (Figure 2b), high-resolution TEM (HRTEM) image and the corresponding fast Fourier transform (FFT) patterns (Figure 2c), XRD pattern together with Raman spectrum (Figures S5 and S6), jointly demonstrate that the core and shell were composed of cubic Cu and wurtzite CdS, respectively.

Moreover, as displayed in Figure 2d, the Cu 2p X-ray photon spectroscopy (XPS) and Cu LMM Auger spectra of the obtained Cu@CdS indicate that the CdS shell is doped with Cu^{+} impurities,[49] due to the incomplete conversion during the cation exchange process. This led to the p-type conductivity for the shell in Cu@CdS as revealed by the open-circuit potential measurement (Figure 2e).[50,51] Therefore, it is expected that the CdS shell could favorably accept the hot holes generated from the LSPR of the Cu core.[52–54] According to Figure 2f, Cu@CdS well combines the absorption features of both CdS and Cu (LSPR band centered at 600 nm), giving rise to broadband light capture across the UV–vis region, which is highly advantageous in the context of conducting photoredox organic synthesis using sunlight. Besides, aside from Cu@CdS, a variety of Cu@MS_x (M = Sn, Ni, Co, Mn, In, Zn) core@shell triangular prisms could be readily accessed by employing the same synthetic strategy (Figure S7; Tables S1 and S2), offering a versatile platform for exploring the great potential of plasmonic Cu-based catalysts.

Reaction Optimization and Substrate Scope Development

The heterobiaryl coupling of 4′-bromoacetophenone (**1a**) with *N*-methylpyrrole (**2a**) was selected as a model reaction to investigate the performance of Cu@CdS as a heterogeneous photoredox catalyst. At first, a xenon lamp equipped with an

Table 1: Evaluation of reaction conditions.

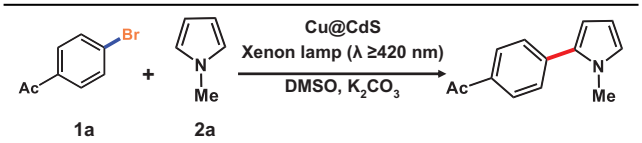

1a 2a

Entry	Modifications of reaction conditions	Yield of 3a (%)[b]
1	**None**[a]	**87**
2	**No catalyst**	**8**
3	**Without light**	**<1**
4	**90 °C without light**[c]	**0**
5	**120 °C without light**[c]	**2**
6	**Under air atmosphere**	**30**
7	**Cu**	**10**
8	**Cu@Cu_2O**	**Trace**
9	**CdS**[d]	**34**
10	**Li_2S (homogeneous)**[e]	**90**

[a] Reaction condition: **1a** (0.5 mmol), **2a** (20.0 equiv), Cu@CdS catalyst (10 mol% per S atom), K_2CO_3 (1.5 equiv), DMSO (2.5 mL), xenon lamp (λ ≥420 nm), under N_2, 3 h. [b] ^{1}HNMR yields based on the internal standard. [c] Using external heating. [d] CdS as a heterogeneous catalyst (10 mol% per S atom). [e] Li_2S as a homogeneous catalyst (generating polysulfide anions $S_3^{\bullet-}$ and S_4^{2-}, 10 mol% per S atom). Here, 10 mol% per S atom refers to the molar ratio of the S atoms in the catalyst relative to substrate **1a**.

optical cutoff filter (λ ≥420 nm, 1.2 W cm^{-2}) was used as the light source, and the reaction was performed in DMSO using K_2CO_3 as a buffer under a nitrogen atmosphere at room temperature.[43] As listed in Table 1, the use of Cu@CdS as a catalyst led to efficient conversion of **1a** within 3 h to produce **3a** in 87% yield (Table 1, entry 1, Figure S8). The control experiment showed that in the absence of Cu@CdS, the yield of **3a** sharply decreased to 8% (Table 1, entry 2), and a positive correlation between the amount of Cu@CdS and the generated **3a** was observed (Figure S9), which confirmed the essential role of Cu@CdS for realization of productive cross-coupling. Light irradiation was also demonstrated to be indispensable for the reaction, as the exclusion of light resulted in <1% yield (Table 1, entry 3). It was noticed that upon light irradiation, the temperature of the reaction system increased rapidly and then remained at ~90 °C (Figure S10). To distinguish the influence from thermal energy, the reaction was also carried out at 90 °C by virtue of external heating without light irradiation. No reaction was observed in this condition (Table 1, entry 4), and further enhancing the reaction temperature to 120 °C only produced **3a** in 2% yield (Table 1, entry 5). Based on these findings, it is rational to conclude that the reaction was principally driven by light instead of heat. In addition, the presence of air obviously hampered the reaction (Table 1, entry 6).

When directly using Cu triangular prisms as the catalyst, a low yield of 10% was obtained (Table 1, entry 7), while enclosing the Cu prisms with a Cu_2O shell basically gave no product (Table 1, entry 8, Figure S11). In contrast, the Cu@MS_x (M = Sn, Ni, Co, Mn, In, Zn) core@shell catalysts with a sulfide shell matrix all enabled generation of the desired product **3a**, although in lower yields than Cu@CdS (Figure S12), suggesting that sulfides were critical for the reaction process. Nevertheless, the exclusive use of sulfides, specifically CdS as a catalyst, considerably reduced the formation amount of **3a** relative to Cu@CdS (Table 1, entry 9). This manifested the evident advantage of integration of sulfides with plasmonic Cu to attain enhanced catalytic activity. Apart from the above discussed heterogeneous catalysts, we also performed the reaction using Li_2S as the homogenous photoredox catalyst (giving birth to polysulfide anions $S_3^{\bullet-}$ and S_4^{2-}),[43] which provided **3a** in 90% yield (Table 1, entry 10). These outcomes are encouraging, seeing that the heterogeneous Cu@CdS can afford competitive performance compared to its homogeneous counterpart Li_2S in biaryl cross-coupling reaction (87% vs. 90% at 10 mol% per S atom).

We then explored the scope of the Cu@CdS-catalyzed reaction toward other aryl/heteroaryl halide substrates, including a variety of aryl chlorides having strong and reductively inert C─Cl bonds (Scheme 1, detailed conditions see Table S3). The results showed that 4′-chloroacetophenone (**1b**) and 5-chloro-1-indanone (**1c**) can be converted to the corresponding coupling products in 64% and 55% yields, respectively. Moreover, the reaction of 4-chlorobenzophenone (**1d**) gave rise to an excellent yield of 89%. These findings dictate that Cu@CdS composed a powerful photocatalytic system capable of activating stubborn chloride substrates with high bond dissociation energy (327 kJ mol^{-1} for C(sp^2)─Cl bond).[17,27] As for the aryl/heteroaryl bromides, various functionalized haloarenes bearing polar-π electron withdrawing moieties such as ketone (**1e**–**1g**), aldehyde (**1h**, **1i**) and nitrile (**1j**) reacted well over Cu@CdS heterogeneous catalyst. Aryl bromides bearing electron-donating groups, such as 4-bromotoluene and 4-bromoanisole, were found not suitable for this reaction, probably owing to their more negative reduction potentials. The five-membered ring heteroaryl bromides based on furan (**1k**) and thiophene (**1l**, **1m**), as well as the six-membered ring heteroaryl bromides like pyridine (**1n**, **1o**) and quinolone (**1p**), were all amenable substrates in the Cu@CdS-catalyzed process, demonstrating good functional group tolerance. Also, we observed that the polyhalogenated aromatic substrates can be engaged in the cross-coupling reaction. For example, the reaction of 2-bromo-4-chlorobenzaldehyde (**1q**) was effective in a chemoselective manner at the C─Br bond. When it came to 3,5-dibromobenzonitrile (**1r**), difunctionalization at both of the C─Br bonds occurred predominantly, rather than single functionalization as reported for the homogenous catalyst Li_2S.[43] Besides, the unprotected N─H pyrrole (**2b**) also brought about a good yield of 81%.

Next, we further studied the synthetic applicability of this Cu@CdS heterogeneous catalyst toward borylation and hydrodehalogenation of aryl halides under visible light. The borylation reaction was carried out using bis(pinacolato)diboron (B_2pin_2) and tetramethylguanidine (TMG) as the radical trapping reagent and base, respectively. It was found that pinacol arylboronate can be obtained in 66% yield, and the reaction protocol was also

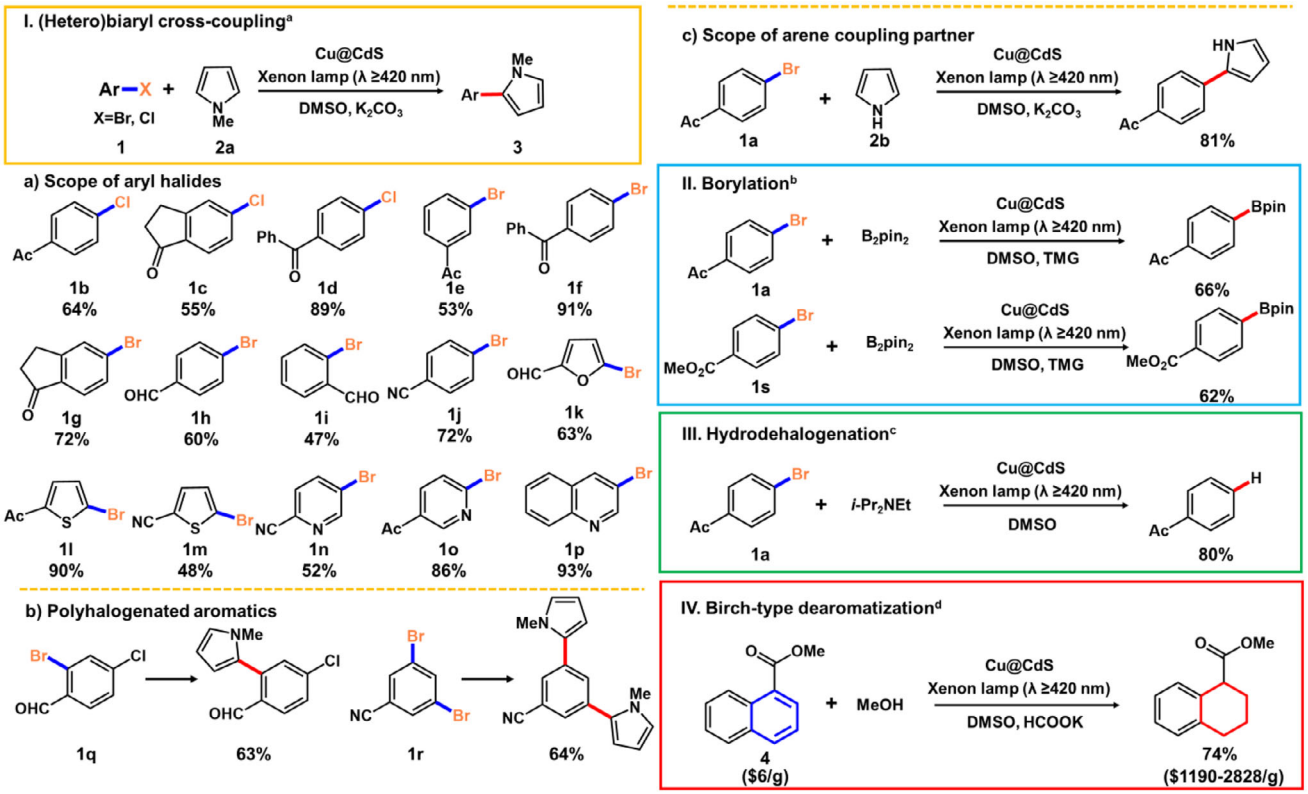

Scheme 1. Reaction scope of Cu@CdS for photoredox reactions. [a]Reaction condition: **1a** (0.5 mmol), **2a** (20.0 equiv), Cu@CdS catalyst (10 mol% per S atom), K_2CO_3 (1.5 equiv), DMSO (2.5 mL), xenon lamp (λ ≥420 nm), under N_2, 3–7 h (Table S3). [b]Reaction condition: **1a** or **1s** (0.5 mmol), B_2pin_2 (20 equiv), Cu@CdS catalyst (10 mol% per S atom), TMG (1.5 equiv), DMSO (2.5 mL), xenon lamp (λ ≥420 nm), under N_2, 4 or 6 h (Table S3). [c]Reaction condition: **1a** (0.5 mmol), *i*-Pr_2NEt (20 equiv), Cu@CdS catalyst (10 mol% per S atom), DMSO (2.5 mL), xenon lamp (λ ≥420 nm), under N_2, 3 h. [d]Reaction condition: **4** (0.5 mmol), MeOH (20.0 equiv), Cu@CdS catalyst (10 mol% per S atom), HCOOK (5.0 equiv), DMSO (2.5 mL), xenon lamp (λ ≥420 nm), under N_2, 7 h.

adaptable to the borylation of functionalized haloarenes such as 4-bromobenzoate (**1s**). Meanwhile, by employing diisopropylethylamine (*i*-Pr_2NEt) as a hydrogen donor, the hydrodebromination of **1a** proceeded smoothly, delivering acetophenone in 80% yield.

To our delight, we found that Cu@CdS also facilitated efficient Birch-type dearomatization of arenes under visible light irradiation. This type of reaction is crucial for the pharmaceutical industry because of its ability to transform readily accessible two-dimensional planar arenes to three-dimensional C(sp^3)-rich aliphatic scaffolds.[41] Typically, the reaction demands use of a super-stoichiometric amount of pyrophoric alkali metals such as lithium or sodium at cryogenic temperatures lower than −33 °C.[55] Encouraged by the lately achieved progress by Tan et al. using polysulfide anions as the photoredox catalyst,[41] we conducted the dearomatization reaction at ambient conditions in DMSO with MeOH and HCOOK as proton and electron donors, respectively. Employing methyl 1-naphthoate (**4**) as a model substrate, we observed that under λ ≥420 nm visible light irradiation, Cu@CdS successfully achieved photocatalytic dearomatization of inexpensive **4** ($6 per g, Aladdin), generating high-value added tetrahydronaphthalene (~$1190–2828 per g, Table S4) in 74% yield as a sole product.

Natural Sunlight-Driven Aryl Cross-Coupling Reaction

After identifying the good efficiency and broad utility of Cu@CdS under xenon lamp irradiation, we set out to determine its photoredox performance, exploiting outdoor solar light as the illumination source. The setup of the reaction system is presented in Figure 3a, where a convex lens (330–2100 nm) with a diameter of 10 cm was placed on top of the reaction tube to concentrate sunlight. On a typical sunny day in Beijing, the power density of the natural sunlight was changed to around ~120 mW cm^{-2} during midnoon, and it can be increased to ~1200 mW cm^{-2} by means of the convex lens (Figure 3b). In this condition, the Cu@CdS-catalyzed coupling between **1a** and **2a** achieved a 77% yield in 3 h (Figure 3c), close to that obtained by using an artificial xenon lamp (Figure 3d). This markedly outperformed CdS, which produced **3a** in a low yield of 10% after 3 h exposure to the concentrated sunlight (Figure 3d). Aside from **1a**, Cu@CdS also displayed remarkable capability for reduction of 4-bromobenzophenone (**1f**), 5-bromo-1-indanone (**1g**), as well as 2-acetyl-5-bromothiophene (**1l**) under concentrated sunlight, resulting in corresponding coupling products in 90%, 63%, and 84% yields within 3 h (Figure 3c). These results substantiate the great potential of Cu@CdS in the synthesis

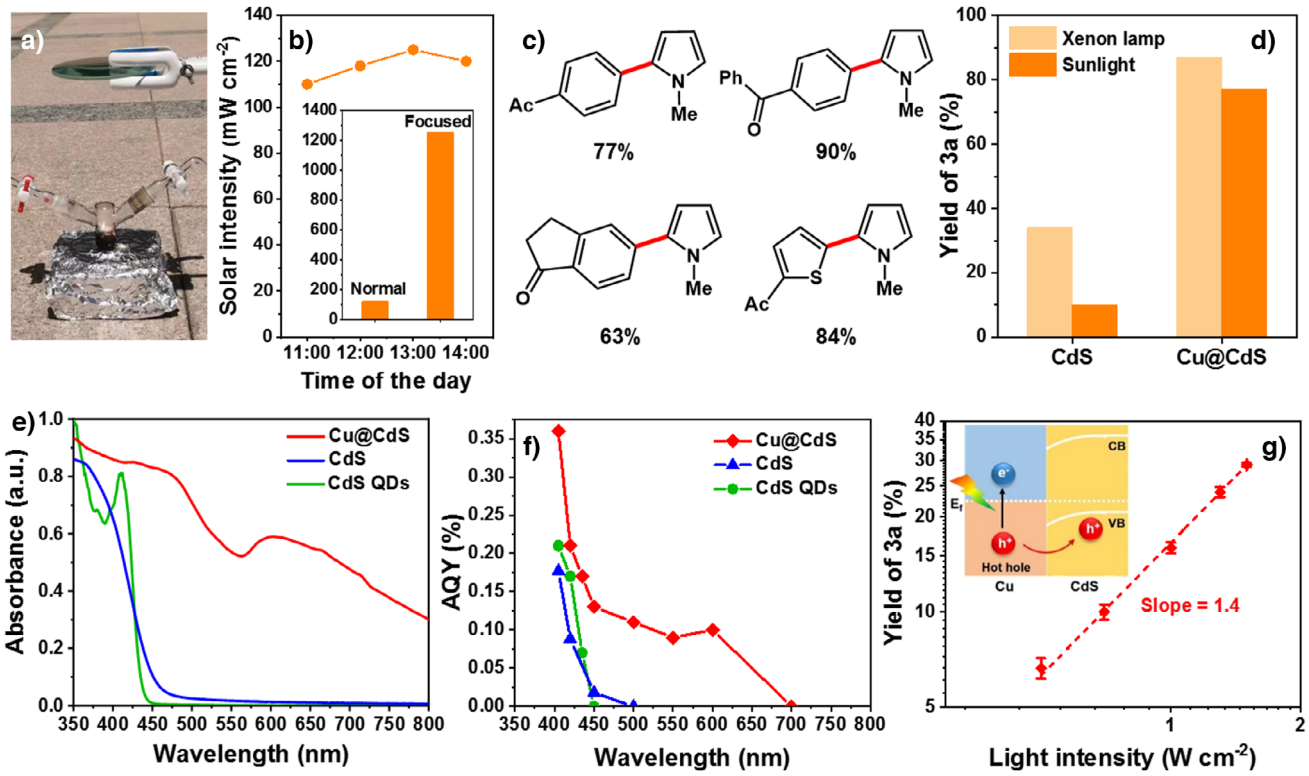

Figure 3. Natural sunlight-driven photoredox reactions over Cu@CdS. a) Photograph of the reaction setup under outdoor sunlight irradiation. b) Variation of the solar intensity with time during the outdoor reaction (inset: the averaged solar intensity before and after the use of a convex lens). c) The yields obtained for various products in biaryl cross-coupling reactions using natural sunlight as an energy source. Reactions condition: **1** (**1a**, **1f**, **1g**, or **1l**, 0.5 mmol), **2a** (20.0 equiv), Cu@CdS catalyst (10 mol% per S atom), K_2CO_3 (1.5 equiv), DMSO (2.5 mL), concentrated outdoor sunlight, under N_2, 3 h. d) Comparison of the yields of **3a** under a xenon lamp ($\lambda \geq 420$ nm) and concentrated natural sunlight for CdS and Cu@CdS. e) Comparison of the optical absorption spectra for Cu@CdS, CdS (bulk), and CdS QDs. f) Wavelength-dependent AQY for Cu@CdS, CdS (bulk), and CdS QDs in cross-coupling reaction between **1a** and **2a**. g) The yield of **3a** as a function of light intensity over Cu@CdS after 1 h of reaction (inset: illustration of hot hole injection in Cu@CdS when plasmonic Cu is excited), where error bars are determined based on three independent experiments.

of complex targeted molecules through straightforwardly harnessing the natural sunlight as a renewable source.

The notably enhanced performance observed for Cu@CdS relative to CdS in the coupling reaction, both under xenon lamp and sunlight irradiation, was considered to have arisen from its broadband light absorption contributed by the LSPR of the Cu component. To verify this assumption, the absorption spectra of Cu@CdS, CdS (bulk), as well as CdS quantum dots (QDs) that have been intensively exploited as photocatalysts for organic synthesis (Figure S13),[26,31,38,55] were compared in Figure 3e. In sharp contrast to Cu@CdS, CdS alone, either in bulk or quantum dimension, exhibited a narrow visible light response, with absorption edges restricted at 450 and 430 nm, respectively. Meanwhile, the generation of **3a** at a series of monochromatic lights was monitored for the three samples. Based on which the apparent quantum yield (AQY) at each wavelength was calculated (Figure 3f), and the results clearly manifested that the strong visible-light harvesting of Cu@CdS was able to deliver photoredox activity beyond the absorption threshold of CdS. We further measured the production of **3a** over Cu@CdS as a function of the intensity of visible illumination. From Figure 3g, a super-linear power-law dependency was observed ($\propto$intensity^n, $n = 1.4$). This has been proposed to be a signature of plasmon-mediated chemical conversion,[56–60] suggesting that the plasmonic hot holes generated upon excitation of the Cu core might play an important part in the cross-coupling reaction by injection into the p-type CdS shell.[52–54]

Investigation on Surface Reactive Species and Reaction Mechanism

To acquire more in-depth insights into the reaction mechanism, the electronic band structure of CdS was evaluated by ultraviolet photo-electron spectroscopy ([UPS], Figure S14). The results indicated that the conduction band (CB) of CdS was at −1.03 V vs. SCE, which means the reduction of **1a** ($E_{red} = -1.89$ V vs. SCE) based on the CB of CdS was thermodynamically unfavorable.[43] In other words, the reaction processes observed in our study should be beyond the conventional mode proposed for semiconductor photoredox catalysts, where photogenerated electrons (holes) in CB (VB) account for the reduction (oxidation) of organic substrates.[59,60] This led us to explore other possible mechanisms that can offset the insufficient energy input for reducing

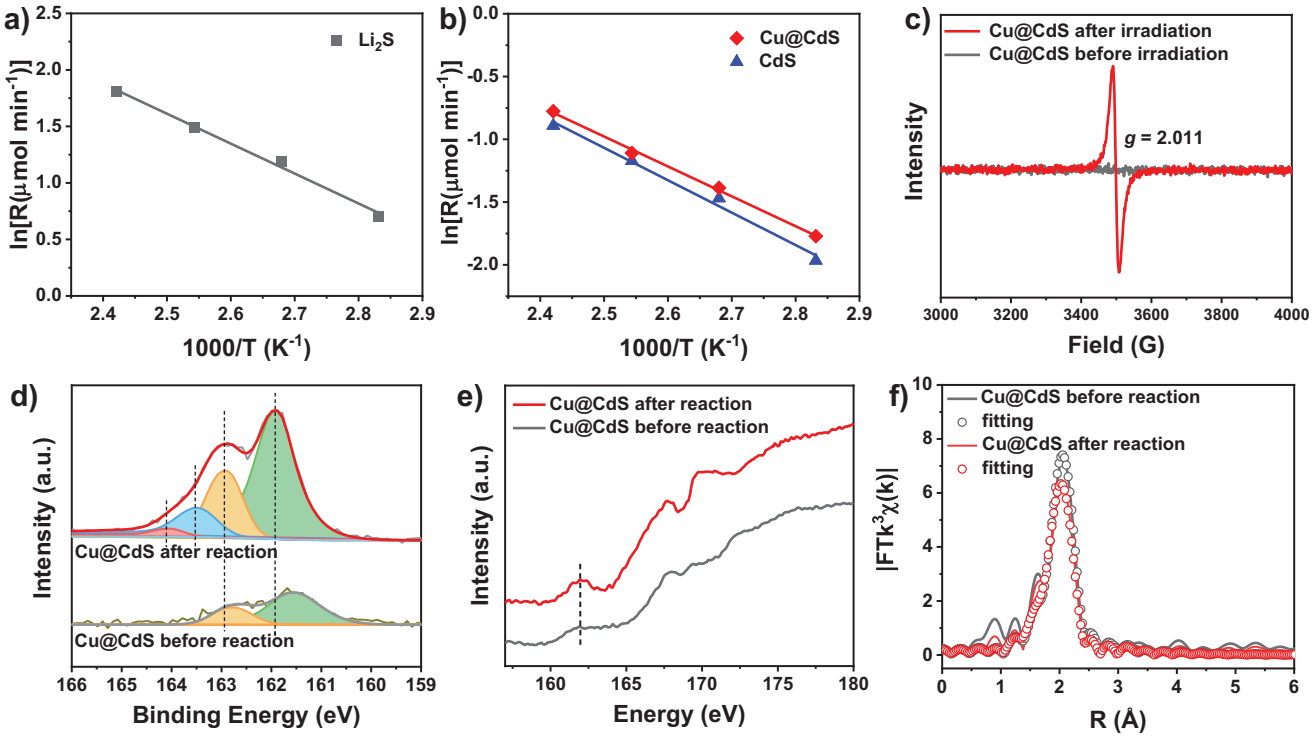

Figure 4. Determination of surface reactive species over Cu@CdS. a), b) Arrhenius plots for cross-coupling reaction between **1a** and **2a** over homogeneous Li_2S photocatalyst a) as well as heterogeneous Cu@CdS and CdS b). c) EPR spectra for Cu@CdS before and after λ ≥420 nm visible light illumination for 20 min. d), e), and f) S 2p XPS spectra d), S L-edge XANES spectra e), Cd K-edge FT-EXAFS spectra with corresponding fitting curves f) for Cu@CdS before and after the coupling reaction between **1a** and **2a** under λ ≥420 nm visible light irradiation.

1a and other challenging substrates. Previously reported strategies employing two photons in one catalytic cycle, either based on ConPET or SenI-ET,[2,13,18,38] can be excluded as no electron donor reagents like trimethylamine (Et_3N), tris(2-aminoethyl)amine (TAEA), and *N*,*N*-diisopropylethylamine (DIPEA) were introduced in our reaction system. The mechanism involving TTA-UC is also implausible under our reaction conditions due to the absence of electron donors, triplet acceptor ligands, as well as annihilator molecules.[19,20]

Intriguingly, as presented in Figure 4a,b, we found that with regard to the coupling reaction of **1a** and **2a**, the apparent activation energy (E_a) for homogeneous catalyst Li_2S under λ ≥420 nm visible light irradiation was 22.0 kJ mol^{-1}, which was very close to those determined for CdS and Cu@CdS at 21.5 and 19.1 kJ mol^{-1}, correspondingly (details see Figures S15–S17). These outcomes implicated that the latter two heterogeneous catalysts might possess a similar reaction pathway to that of Li_2S, which correlates with the high redox power of polysulfide anions $S_3^{\bullet-}$ and S_4^{2-} upon visible-light excitation. Such a mechanism could be pertinent to our heterogeneous reaction system, in consideration of the facile oxidation of S^{2-} in the CdS component caused by photogenerated holes, principally enabling the generation of polysulfide species over CdS. However, currently the prevalent view is that photocorrosion of metal sulfides gives rise to SO_4^{2-} or S^0 in the environment containing oxygen or not, respectively.[61] Other products that could be formed in the photocorrosion process have been less well studied.

To discern whether polysulfide species could be formed and operative in our system, first, electron paramagnetic resonance (EPR) spectra were collected over Cu@CdS before and after illumination with λ ≥420 nm visible light for 20 min (Figure 4c). A notable signal at $g = 2.011$ was observed after irradiation. The *g* value was identical with that reported for the trapped hole at S^{2-} in irradiated ZnS,[62] i.e., the $S^{\bullet-}$ radical ion.[63,64] Next, XPS was applied to determine the existence of polysulfide species over Cu@CdS during the cross-coupling reaction between **1a** and **2a** under visible light (Figures 4d and S18). As exhibited in Figure 4d, the S $2p_{3/2}$ (161.5 eV) and S $2p_{1/2}$ (162.8 eV) peaks characteristic of S^{2-} in CdS shifted to higher binding energies after undergoing the reaction,[65] revealing a reduced electron density. More importantly, two new peaks at 163.5 and 164.0 eV emerged after the reaction, which have been assigned to $S_3^{\bullet-}$ and S_4 species, respectively, in previous studies.[66] The above findings are in good agreement with the variation in S L-edge X-ray absorption near-edge structure (XANES) spectra observed for Cu@CdS before and after the coupling reaction (Figure 4e). That is, the intensity of the pre-edge peak was enhanced after the reaction, where the peak intensity has been proposed to be indicative of the content of polymeric sulfur species containing S—S bonds.[67,68] In addition to S element, the local coordination environment of Cd atoms in Cu@CdS was also examined with X-ray absorption spectroscopy (Figures 4f and S19–S21; Table S5). Figure 4f presents the Fourier-transformed extended X-ray absorption

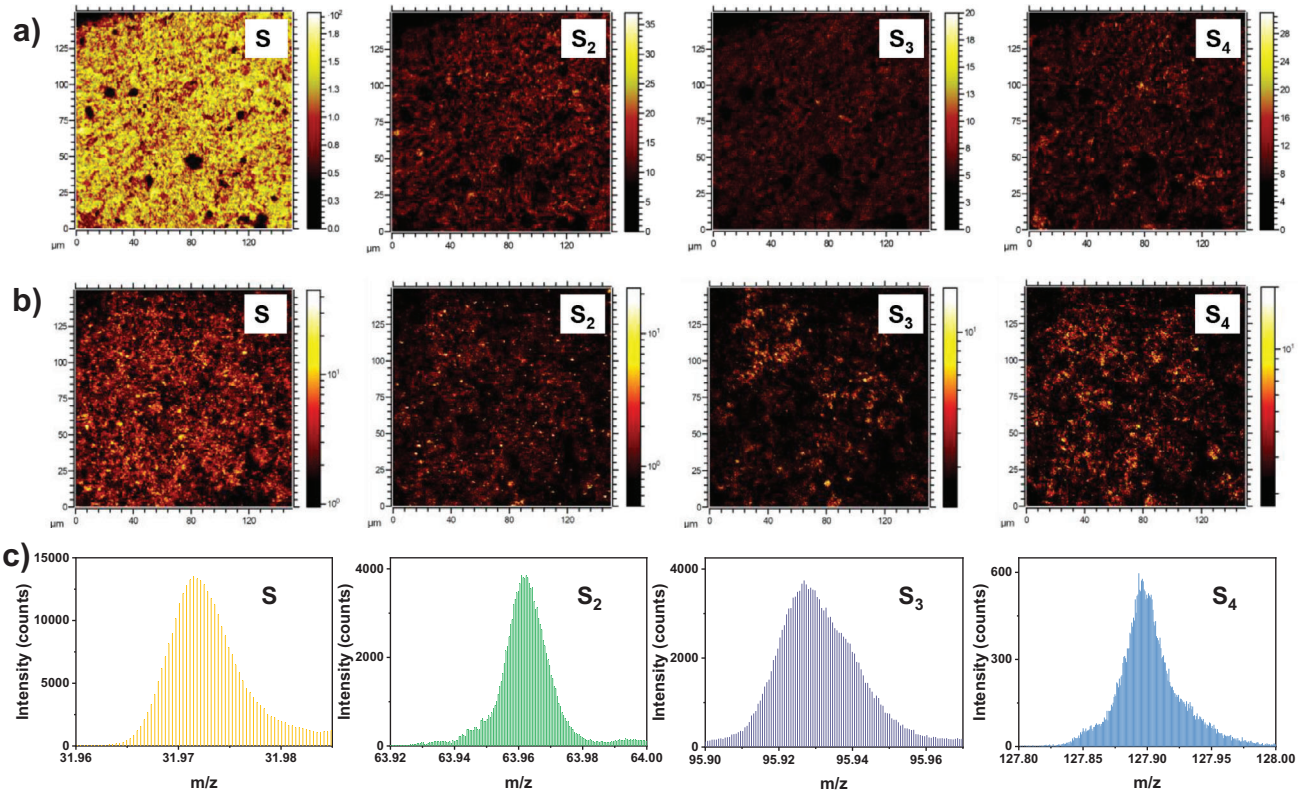

Figure 5. Evolution of polysulfide species over Cu@CdS under visible light irradiation. a) TOF-SIMS mapping images of Cu@CdS after exposure to visible light irradiation (λ ≥420 nm) for 20 min. b), c) TOF-SIMS mapping images b) and corresponding mass spectra c) of Cu@CdS after exposure to visible light irradiation (λ ≥420 nm) for 60 min.

fine structure (FT-EXAFS) spectra and corresponding fitting curves at Cd K-edge for Cu@CdS before and after the reaction. The fitting parameters disclosed that the coordination number of Cd—S decreased from 3.8 to 3.1 after the reaction (Table S5), suggesting the cleavage of Cd—S bonds and the resulting opportunities for the formation of polysulfides during the reaction process.

Time-of-flight secondary ion mass spectrometry (TOF-SIMS) was further exploited to acquire more direct evidence on the formation and evolution of polysulfides. From Figures 5a and S22, one can see that after 20 min of visible light exposure, S_2, S_3, and S_4 species were detected on the surface of Cu@CdS in addition to the main component S. The concentrations of the generated polysulfides were increased when the irradiation time was extended to 60 min (Figures 5b,c, and S23). The presence of S_2, S_3, and S_4 was also observed for visible light-irradiated CdS, though with much reduced concentrations in comparison with those of Cu@CdS under the same conditions (Figures S24 and S25). From the above results, we infer that linked sulfur in the form of short chains might be generally produced during the photocorrosion process of CdS photocatalysts.

Taken together, the above obtained information unambiguously demonstrated that polysulfide species S_n with $n = 2$–4 could be formed on Cu@CdS by illumination with visible light. During this process, the $S^{\bullet-}$ anion is considered to be the first intermediate, produced most likely as a result of the trapped holes at the CdS surface, according to the reports of Kamat and Stucky (Equation 1).[63,69,70]

$$S^{2-} + h^+ \rightarrow S^{\bullet-} \quad (1)$$

The formed $S^{\bullet-}$ anions are prone to be annihilated with each other, giving birth to S_2^{2-} via Equation (2) ($\Delta_r G^\theta{}_m = -176$ kJ mol^{-1}, 298 K): [71,72]

$$2S^{\bullet-} \rightarrow S_2^{2-} \quad (2)$$

$$S_2^{2-} + h^+ \rightarrow S_2^{\bullet-} \quad (3)$$

The further oxidation of S_2^{2-} by photogenerated holes is thermodynamically favorable with a substantial reduction in Gibbs free energy via Equation (3) ($\Delta_r G^\theta{}_m = -354$ kJ mol^{-1}, 298 K), and the resulting $S_2^{\bullet-}$ can exothermically form S_4^{2-} via Equation (4) ($\Delta_r G^\theta{}_m = -87$ kJ mol^{-1}, 298 K): [72]

$$2S_2^{\bullet-} \rightarrow S_4^{2-} \quad (4)$$

Meanwhile, the $S^{\bullet-}$ intermediate can also couple with two neighboring S^{2-} leading to $S_3^{\bullet-}$ radical anion via Equation (5):[73]

$$S^{\bullet-} + 2S^{2-} \rightarrow S_3^{\bullet-} \quad (5)$$

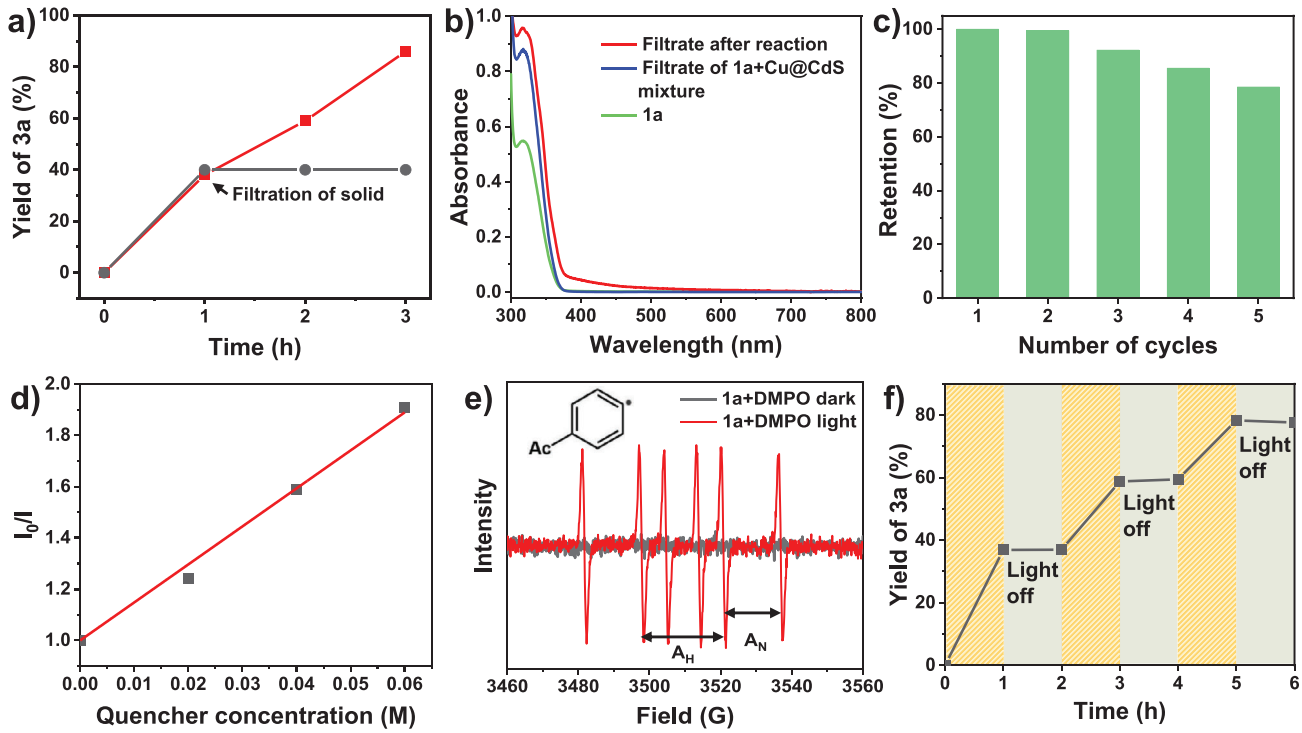

Figure 6. Verification of heterogeneous radical-mediated mechanism for Cu@CdS. a) Time-dependent evolution of **3a** with (dark grey line) and without (red line) removal of the solid catalyst Cu@CdS at 1 h during the coupling reaction of **1a** and **2a**. b) UV–vis spectra for **1a** in DMSO, the filtrate collected from the DMSO solution of **1a** and Cu@CdS after mixing for 3 h, as well as the filtrate obtained by removing the solid catalyst Cu@CdS from the coupling reaction system after 3 h. c) Recycling performance of Cu@CdS in coupling reaction of **1a** and **2a**. d) Stern–Volmer plot with **1a** as quencher. e) EPR spin-trapping experiment by introducing DMPO into the coupling reaction system ($g = 2.002$, AN = 16 G, AH = 23 G). f) Yield of **3a** under light on/off conditions in the coupling reaction over Cu@CdS.

On the basis of these reaction pathways, we propose that the $S_3^{\bullet-}$ and S_4^{2-} anions are feasible to be produced on the surface of Cu@CdS by leveraging the photocorrosion of CdS during photoinduced reactions, in which the plasmonic hot holes injected from Cu probably make a significant contribution. As discussed above, such surface polysulfide spots could serve as potent photoredox active sites after being excited by visible light to elicit challenging potentials and engage in a myriad of synthetically valuable transformations. It should be pointed out that although other polysulfide species like $S_2^{\bullet-}$ (λ_{max} = 400 nm), S_3^{2-} (λ_{max} = 273 nm), and $S_4^{\bullet-}$ (λ_{max} = 350 and 998 nm) could be formed in accompaniment with $S_3^{\bullet-}$ and S_4^{2-},[74] they cannot efficiently absorb visible light and thus may not cause notable impacts on the photoredox process.

As presented in Figure 6a, the hot filtration experiment uncovered that after removal of the solid catalyst Cu@CdS by filtration at 1 h, the coupling reaction between **1a** and **2a** completely ceased with the yield of **3a** unchanged during the following 2 h. Moreover, the filtrate collected after 3 h of reaction under standard conditions showed no absorption peaks in the region from 430 to 800 nm that can be ascribed to $S_3^{\bullet-}$ (λ_{max} = 618 nm) and S_4^{2-} (λ_{max} = 436 nm) anions dissolved in DMSO (Figure 6b). Also, the filtrate of a mixture of **1a** and Cu@CdS (stirring for 3 h) demonstrated that no S^{2-} ions leached out from the Cu@CdS solids (Figure 6b), different from the mechanism reported for homogenous S^{2-} which formed an electron-donor-acceptor (EDA) complex with **1a** to absorb visible light.[43] Inductively coupled plasma-atomic emission spectrometry (ICP-AES) and CHNS elemental analysis (EA) measurements further indicated that after the coupling reaction, the content of sulfur in Cu@CdS was unreduced (Table S6). Combinations of the above outcomes strongly confirmed the heterogeneous nature of the photoredox process catalyzed by Cu@CdS. The superiority of such heterogeneous system over the homogeneous polysulfide anions was underscored by the good reusability observed for Cu@CdS. As shown in Figure 6c, about 80% of its initial conversion efficiency can be retained after five consecutive cycles. The recycled catalyst exhibited good structural integrity according to TEM and XRD characterizations (Figure S26). We conjecture that loss of catalyst amount during the recycling process might be a major reason leading to the slight decrease in activity.

Similar to the catalytic mode of homogeneous $S_3^{\bullet-}$ and S_4^{2-} couples, we propose that heterogeneous Cu@CdS also entails the SET-driven radical-mediated events in aryl cross-coupling reactions. Specifically, Stern–Volmer luminescence quenching experiments suggested that substrate **1a** can quench the excited state of the heterogeneous photocatalyst via electron transfer in our case (Figures 6d and S27, here CdS QDs were studied as Cu@CdS showed no luminescence, energy transfer was unlikely due to the lack of spectrum and orbital overlap).[75] Besides, a

radical pathway was demonstrated by inhibition of the coupling reaction upon introducing the radical scavengers TEMPO (2,2,6,6-tetramethylpiperidinooxy) or BHT (butylated hydroxytoluene) into the reaction mixture (Table S7). EPR spin-trapping experiments with DMPO (5,5-dimethyl-1-pyrroline-N-oxide) further unveiled that aryl radical was the key radical intermediate (Figure 6e). Besides, the light on/off control experiments exhibited in Figure 6f signified the low possibility of the occurrence of radical chain reactions.[29,76]

Given the information gleaned above, an integral catalytic profile can be presumed, as illustrated in Figure 1d.[42,43] Plasmonic Cu prisms interacting with a wide range of visible light serve as a significant light absorber in Cu@CdS to convert photon energy into energetic electrons and holes. The generated holes can form $S_3^{\bullet-}$ and S_4^{2-} species on the surface of the CdS shell through the processes described in Equations (1) to (5). Photoexcitation by blue light imparts the S_4^{2-} sites with a highly reducing potential. Taking the reaction between **1a** and **2a** as an example, this enables reduction of substrate **1a** via SET followed by mesolysis of C─Br bond to give the corresponding aryl radical, along with concurrent oxidation of excited S_4^{2-} into $S_4^{\bullet-}$. The yielded aryl radical then adds onto substrate **2a**. The resultant dearomatized radical intermediate undergoes single-electron oxidation induced by the red light-excited $S_3^{\bullet-}$ as well as subsequent deprotonation, liberating the final product **3a** accompanied by the formation of S_3^{2-}. Photoexcited electrons and holes in Cu@CdS regenerate S_4^{2-} and $S_3^{\bullet-}$ via reduction of $S_4^{\bullet-}$ and oxidation of S_3^{2-}, respectively, thereby accomplishing the photoredox catalytic cycle.

Conclusion

In this work, a new type of photoredox catalyst has been created via integrating plasmonic Cu and CdS into a core@shell structure as well as building polysulfide species on the CdS surface by leveraging photocorrosion. The Cu core played the part of antenna to efficiently harvest visible light, while the polysulfide species, such as $S_3^{\bullet-}$ and S_4^{2-}, in their excited state can function as powerful redox catalytic sites to induce SET-driven radical-mediated reactions. Beneficial from such catalyst design, the natural sunlight can be directly harnessed to productively synthesize various complex organic molecules in a manner with operational and practical advantages. The findings presented here may offer an interesting prototype for research efforts in the direction of realizing Ciamician's prophetic vision of solar manufacturing. Moreover, the recognition of the unique reactivity of surficial polysulfide species could be enlightening for the rational design of the next generation of chalcogenide photocatalytic systems.

Acknowledgements

This work was supported by the National Natural Science Foundation of China (Grant No. 52072035, 52272186, 22301299), Dalian Institute of Chemical Physics (DICP I202423).

Conflict of Interests

The authors declare no conflict of interest.

Data Availability Statement

The data that support the findings of this study are available from the corresponding author upon reasonable request.

Keywords: Photocatalysis · Photoredox catalyst · Polysulfides · Solar synthesis · Surface plasmon resonance

[1] G. Ciamician, *Science* **1912**, *36*, 385–394.
[2] I. Ghosh, T. Ghosh, J. I. Bardagi, B. Koenig, *Science* **2014**, *346*, 725–728.
[3] G. E. M. Crisenza, P. Melchiorre, *Nat. Commun.* **2020**, *11*,803.
[4] D. A. Nicewicz, D. W. C. MacMillan, *Science* **2008**, *322*, 77–80.
[5] S.-L. Meng, C. Ye, X.-B. Li, C.-H. Tung, L.-Z. Wu, *J. Am. Chem. Soc.* **2022**, *144*, 16219–16231.
[6] N. E. S. Tay, D. Lehnherr, T. Rovis, *Chem. Rev.* **2022**, *122*, 2487–2649.
[7] L. Marzo, S. K. Pagire, O. Reiser, B. Koenig, *Angew. Chem. Int. Ed.* **2018**, *57*, 10034–10072.
[8] A. Y. Chan, I. B. Perry, N. B. Bissonnette, B. F. Buksh, G. A. Edwards, L. I. Frye, O. L. Garry, M. N. Lavagnino, B. X. Li, Y. Liang, E. Mao, A. Millet, J. V. Oakley, N. L. Reed, H. A. Sakai, C. P. Seath, D. W. C. MacMillan, *Chem. Rev.* **2022**, *122*, 1485–1542.
[9] J. D. Bell, J. A. Murphy, *Chem. Soc. Rev.* **2021**, *50*, 9540–9685.
[10] J. Märsch, S. Reiter, T. Rittner, R. E. Rodriguez-Lugo, M. Whitfield, D. J. Scott, R. J. Kutta, P. Nuernberger, R. de Vivie-Riedle, R. Wolf *Angew. Chem. Int. Ed. 63*, e202405780.
[11] D. M. Schultz, T. P. Yoon, *Science* **2014**, *343*, 1239176.
[12] M. Oelgemoller, *Chem. Rev.* **2016**, *116*, 9664–9682.
[13] H. Tan, H. J. Li, W. Q. Ji, L. Wang *Angew. Chem. Int. Ed.* **2015**, *54*, 8374–8377.
[14] J. Xie, S. Shi, T. Zhang, N. Mehrkens, M. Rudolph, A. S. K. Hashmi,*Angew. Chem. Int. Ed.* **2015**, *54*, 6046–6050.
[15] D. L. Zhu, S. J. Qi, W. H. Wang, L. L. Chai, H. Y. Li, H. X. Li, *Org. Lett.* **2021**, *23*, 160–165.
[16] T. Yuan, L. Sun, Z. Wu, R. Wang, X. Cai, W. Lin, M. Zheng, X. Wang, *Nat. Catal.* **2022**, *5*, 1157–1168.
[17] X. Tian, Y. Liu, S. Yakubov, J. Schuette, S. Chiba, J. P. Barham, *Chem. Soc. Rev.* **2024**, *53*, 263–316.
[18] A. Chatterjee, B. Koenig, *Angew. Chem. Int. Ed.* **2019**, *58*, 14289–14294.
[19] W. Liang, C. Nie, J. Du, Y. Han, G. Zhao, F. Yang, G. Liang, K. Wu, *Nat. Photonics* **2023**, *17*, 346–353.
[20] B. D. Ravetz, A. B. Pun, E. M. Churchill, D. N. Congreve, T. Rovis, L. M. Campos, *Nature* **2019**, *565*, 343–346.
[21] M. Cybularczyk-Cecotka, J. Szczepanik, M. Giedyk, *Nat. Catal.* **2020**, *3*, 872–886.
[22] F. Glaser, C. Kerzig, O. S. Wenger, *Angew. Chem. Int. Ed.* **2020**, *59*, 10266–10284.
[23] L. Zeng, L. Huang, W. Lin, L. H. Jiang, G. Han, *Nat. Commun.* **2023**, *14*, 1102.
[24] J. Xu, J. Cao, X. Wu, H. Wang, X. Yang, X. Tang, J. Wu, *J. Am. Chem. Soc.* **2021**, *143*, 13266–13273.
[25] H. Zhao, V. D. Cuomo, W. Tian, C. Romano, D. J. Procter, *Nat. Rev. Chem.* **2025**, *9*, 61–80.
[26] K. Wu, L.-Z. Wu, *Chem* **2021**, *7*, 842–844.
[27] Q. Yang, X. Li, L. Chen, X. Han, F. R. Wang, J. Tang, *Angew. Chem. Int. Ed.* **2023**, *62*, e202307907.

[28] A. Savateev, M. Antonietti, *ACS Catal.* **2018**, *8*, 9790–9808.
[29] G. Wang, Y. Liu, X. Zhang, X. Zong, X. Zhang, K. Zheng, D. Qu, L. An, X. Qi, Z. Sun, *J. Am. Chem. Soc.* **2024**, *146*, 8668–8676.
[30] S. Li, W. Wei, K. Chi, C. T. J. Ferguson, Y. Zhao, K. A. I. Zhang, *J. Am. Chem. Soc.* **2024**, *146*, 12386–12394.
[31] Z. Zhang, K. Edme, S. Lian, E. A. Weiss, *J. Am. Chem. Soc.* **2017**, *139*, 4246–4249.
[32] J. A. Caputo, L. C. Frenette, N. Zhao, K. L. Sowers, T. D. Krauss, D. J. Weix, *ACS Catal.* **2023**, *13*, 9018–9024.
[33] X.-B. Li, Z.-J. Li, Y.-J. Gao, Q.-Y. Meng, S. Yu, R. G. Weiss, C.-H. Tung, L.-Z. Wu, *Angew. Chem. Int. Ed.* **2014**, *53*, 2085–2089.
[34] A. Pal, I. Ghosh, S. Sapra, B. Koenig, *Chem. Mater.* **2017**, *29*, 5225–5231.
[35] Q.-C. Gan, J. Qiao, C. Zhou, R.-N. Ci, J.-D. Guo, B. Chen, C.-H. Tung, L.-Z. Wu, *Angew. Chem. Int. Ed.* **2023**, *62*, e202218391.
[36] H. Hao, X. Lang, *ChemCatChem* **2019**, *11*, 1378–1393.
[37] J.-Y. Li, Y.-H. Li, M.-Y. Qi, Q. Lin, Z.-R. Tang, Y.-J. Xu, *ACS Catal.* **2020**, *10*, 6262–6280.
[38] J. K. Widness, D. G. Enny, K. S. McFarlane-Connelly, M. T. Miedenbauer, T. D. Krauss, D. J. Weix, *J. Am. Chem. Soc.* **2022**, *144*, 12229–12246.
[39] D. Liu, A. Hazra, X. Liu, R. Maity, T. Tan, L. Luo, *Angew. Chem. Int. Ed.* **2024**, *63*, e202403186.
[40] C. J. Aschendorf, M. Degbevi, K. V. Prather, E. Y. Tsui, *Chem. Sci.* **2023**, *14*, 13080–13089.
[41] E. Y. K. Tan, A. S. Mat Lani, W. Sow, Y. Liu, H. Li, S. Chiba, *Angew. Chem. Int. Ed.* **2023**, *62*, e20230976.
[42] H. Li, Y. Liu, S. Chiba, *JACS Au* **2021**, *1*, 2121–2129.
[43] H. Li, X. Tang, J. H. Pang, X. Wu, E. K. L. Yeow, J. Wu, S. Chiba, *J. Am. Chem. Soc.* **2021**, *143*, 481–487.
[44] Y. Xin, K. Yue, L. T. Zhang, Y. R. Yang, H. B. Yuan, H. L. Li, L. B. Wang, J. Zeng, *Adv. Mater.* **2021**, *33*, 2008145.
[45] S. Kim, J.-M. Kim, J.-E. Park, J.-M. Nam, *Adv. Mater.* **2018**, *30*, 1704528.
[46] J. Zhang, Y. Tang, K. Lee, O. Min, *Science* **2010**, *327*, 1634–1638.
[47] W. Luc, X. Fu, J. Shi, J.-J. Lv, M. Jouny, B. H. Ko, Y. Xu, Q. Tu, X. Hu, J. Wu, Q. Yue, Y. Liu, F. Jiao, Y. Kang, *Nat. Catal.* **2019**, *2*, 423–430.
[48] X. Wan, Y. Pan, Y. Xu, J. Liu, H. Chen, R. Pan, Y. Zhao, P. Su, Y. Li, X. Zhang, S. Zhang, H. Li, D. Su, Y. Weng, J. Zhang, *Adv. Mater.* **2023**, *35*, 2207555.
[49] H. Li, T. Liu, P. Wei, L. Lin, D. Gao, G. Wang, X. Bao, *Angew. Chem. Int. Ed.* **2021**, *60*, 14329–14333.
[50] R. Pan, J. Liu, Y. Li, X. Li, E. Zhang, Q. Di, M. Su, J. Zhang, *J. Mater. Chem. A* **2019**, *7*, 23038–23045.
[51] J. Kamimura, P. Bogdanoff, M. Ramsteiner, P. Corfdir, F. Feix, L. Geelhaar, H. Riechert, *Nano Lett.* **2017**, *17*, 1529–1537.
[52] S. DuChene, G. Tagliabue, A. J. Welch, X. Li, W.-H. Cheng, H. A. Atwater, *Nano Lett.* **2020**, *20*, 2348–2358.
[53] X. Wan, Y. Gao, M. Eshete, M. Hu, R. Pan, H. Wang, L. Liu, J. Liu, J. Jiang, S. Brovelli, J. Zhang, *Nano Energy* **2022**, *98*, 107217.
[54] S. Bai, J. Jiang, Q. Zhang, Y. Xiong, *Chem. Soc. Rev.* **2015**, *44*, 2893–2939.
[55] C. Huang, X.-B. Li, C.-H. Tung, L.-Z. Wu, *Chem. Eur. J.* **2018**, *24*, 11530–11534.
[56] D. F. Swearer, H. Zhao, L. Zhou, C. Zhang, H. Robatjazi, J. M. P. Martirez, C. M. Krauter, S. Yazdi, M. J. McClain, E. Ringe, E. A. Carter, P. Nordlander, N. J. Halas, *Proc. Natl. Acad. Sci. USA* **2016**, *113*, 8916–8920.
[57] L. Zhou, D. F. Swearer, C. Zhang, H. Robatjazi, H. Zhao, L. Henderson, L. Dong, P. Christopher, E. A. Carter, P. Nordlander, N. J. Halas, *Science* **2018**, *362*, 69–72.
[58] P. Christopher, H. Xin, A. Marimuthu, S. Linic, *Nat. Mater.* **2012**, *11*, 1044–1050.
[59] Y. Yuan, N. Jin, P. Saghy, L. Dube, H. Zhu, O. Chen, *J. Phys. Chem. Lett.* **2021**, *12*, 7180–7193;
[60] H. Kisch, *Acc. Chem. Res.* **2017**, *50*, 1002–1010.
[61] B. Weng, M.-Y. Qi, C. Han, Z.-R. Tang, Y.-J. Xu, *ACS Catal.* **2019**, *9*, 4642–4687.
[62] S. Yanagida, K. Mizumoto, C. Pac, *J. Am. Chem. Soc.* **1986**, *108*, 647–654.
[63] P. V. Kamat, T. W. Ebbesen, N. M. Dimitrijevic, A. J. Nozik, *Chem. Phys. Lett.* **1989**, *157*, 384–389.
[64] D. Meissner, R. Memming, B. Kastening, *J. Phys.Chem.* **1988**, *92*, 3476–3483.
[65] Y. Liu, S. Ding, Y. Shi, X. Liu, Z. Wu, Q. Jiang, T. Zhou, N. Liu, J. Hu, *Appl. Catal. B-Environ.* **2018**, *234*, 109–116.
[66] R. Steudel, T. Chivers, *Chem. Soc. Rev.* **2019**, *48*, 3279–3319.
[67] J. G. Chen, *Surf. Sci. Rep.* **1997**, *30*, 1–152.
[68] Y. Mikhlin, M. Likhatski, Y. Tomashevich, A. Romanchenko, S. Erenburg, S. Trubina, *J. Electron. Spectrosc. Relat. Phenom.* **2010**, *177*, 24–29.
[69] N. C. Strandwitz, A. Khan, S. W. Boettcher, A. A. Mikhailovsky, C. J. Hawker, T.-Q. Nguyen, G. D. Stucky, *J. Am. Chem. Soc.* **2008**, *130*, 8280–8288.
[70] P. V. Kamat, *Chem. Rev.* **1993**, *93*, 267–300.
[71] A. Kumar, E. Janata, A. Henglein, *J. Phys.Chem.* **1988**, *92*, 2587–2591.
[72] X. Li, P. D. McNaughter, P. O'Brien, H. Minamimoto, K. Murakoshi, *J. Phys. Chem. Lett.* **2019**, *10*, 5357–5363.
[73] V. Chakrapani, D. Baker, P. V. Kamat, *J. Am. Chem. Soc.* **2011**, *133*, 9607–9615.
[74] P. Song, W. Rao, T. Chivers, S.-Y. Wang, *Org. Chem. Front.* **2023**, *10*, 3378–3400.
[75] D. M. Arias-Rotondo, J. K. McCusker, *Chem. Soc. Rev.* **2016**, *45*, 5803–5820.
[76] S.-Y. Guo, F. Yang, T.-T. Song, Y.-Q. Guan, X.-T. Min, D.-W. Ji, Y.-C. Hu, Q.-A. Chen, *Nat. Commun.* **2021**, *12*, 6538.

Manuscript received: December 30, 2024
Revised manuscript received: March 31, 2025
Accepted manuscript online: April 24, 2025
Version of record online: ■■, ■■

Research Article

Photocatalysis

Y. Li, S.-Y. Guo, H. Gu, B. Wang, P. Su, X. Zhang, H. Zhang, S. Zhang, F. Yang, J. Liu*, Q.-A. Chen*, J. Zhang* **e202425601**

Natural Sunlight-Driven Activation of Inert Aryl Halides Using Plasmonic Cu@CdS with Polysulfide Active Sites

Chemists have long aspired to construct complex organic compounds the way that plants do by harnessing natural sunlight as an energy source. This study presents an advancement toward this goal via synergistic exploitation of the plasmonic absorption of Cu and the unique redox potentials of excited polysulfide species ($S_3^{\bullet-}$ and S_4^{2-}) on semiconductor surfaces to decouple the thermodynamic limits of photoreduction from photoexcitation.